Chapter 5

Controlling the Alignment of Polyimide for Liquid Crystal Devices

Shie-Chang Jeng and Shug-June Hwang

Additional information is available at the end of the chapter

http://dx.doi.org/10.5772/53457

1. Introduction

Liquid crystal (LC) devices have been popular for use in photonics products, such as displays for mobile phones, televisions and computers. As shown in Fig. 1, a typical LC device consists of a thin LC layer sandwiched between a pair of indium tin oxide (ITO) conducting glass substrates with a cell gap of few micrometers. Polyimide (PI) as a polymeric material characterized by its outstanding mechanical, thermal and electrical properties at moderate high temperature has been widely applied in the LC displays (LCDs) industry as the alignment layers to align LC molecules in a certain orientation and conformation with a specific pretilt angle, the angle between the director of the LC molecules and the PI alignment layer. The pretilt angle is very important and required for LC devices to obtain a defect-free alignment and also to improve their electro-optical performance, such as driving voltage, response time, color performance and viewing angle. However, the applications of conventional PIs in LCDs are limited by a small tuning range of pretilt angle (~ few degrees) either by controlling the rubbing depth or the number of rubbings (Paek et al., 1998).

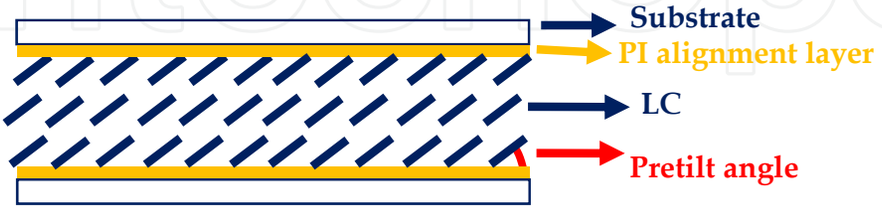

Figure 1. The typical structure of a liquid crystal device.

The pretilt angle of an LCD is either near zero degrees or 90 degrees for using the conventional homogeneous and homeotropic PI materials, respectively. The technique of

producing homogeneous and homeotropic PI is mature in the LCDs industry. For example, the introduction of long alkyl groups into the aromatic diamines has been applied for increasing the pretilt angle from near zero degrees to near 90 degrees (Tsuda, 2011). However, the required specific pretilt angles of LCDs depend on their operation modes, for example, near zero degrees for in-plane switching (displays for iPhone and iPad), several degrees for the twisted nematic mode (displays for Laptop computers), more than 5° for the supertwisted nematic mode, 45^o ~ 60^o for no-bias optically-compensated bend (OCB) mode (LCDs with fast response time and wide viewing angle) and the bi-stable bend-splay (BBS) mode (LCDs requiring memory effect, such as e-books), and near 90 degrees for the vertical alignment mode (LCDs for TVs). Among of them, the OCB LCD has attracted much attention in recent years due to its fast response time and inherent wide view angle property (Acosta et al., 2000), and the memory effect of a bistable LCD is highly suitable for electronic-paper applications due to the low power consumption. The OCB LCD is operated between the bend state and the homeotropic state. A bias voltage should be applied to transfer a conventional OCB mode from the initially splay state to the bend state. Using a high pretilt angle of ~50^o is sufficient to provide a stable bend state in an OCB mode at no bias voltage (Yeung & Kwok, 2006a), and it has been successfully demonstrated to reach the no-bias OCB operation. In general, an alignment layer with a high pretilt angle of around 45^o ~ 58^o is required for a BBS LCD providing the same splay and bend deformation energies (Yu & Kwok, 2004); therefore bistability between bend and splay states are reached.

In order to obtain a demanded pretilt angle for different LCD applications, there are many methods have been developed in the last two decades for controlling the pretilt angle of LC with a wide range, such as: obliquely-evaporated silicon monoxide (Uchida et al., 1980; Janning, 1992), polymer-stabilized alignment (Chen & Chu, 2008), hybrid mixture of two materials (Yeung et al., 2006b; Vaughn et al., 2007; Wu et al., 2008; Ahn et al., 2009), nano-structured surfaces (Komitov, 2008), chemical synthesis (Nishikawa, 2000; Tsuda, 2011), and stacked PI alignment layers (Lee et al., 2009). However, the reliability, the mass production capability and ease of material synthesis for those developed techniques are questionable. For example, the complicate molecular design and synthetic processes are required for a new development of alignment material.

Recently, we have developed a new approach to align LC vertically by adding polyhedral oligomeric silsesquioxane (POSS) nanoparticles in LCDs (Jeng et al., 2007; Hwang et al., 2009). POSS nanoparticles with nano-sized cage structures have been incorporated into polymers for improving their thermal, mechanical and oxidation resistance (Xiao et al., 2003; Yei et al., 2004). A typical structure of the POSS molecule is shown in Fig. 2, with R indicating the functional group (Sigma-Aldrich Corp., St. Louis, MO, USA). In our recent work, we have demonstrated that the pretilt angle of LC molecules can be continuously controlled by using conventional homogeneous PI alignment material doped with different concentrations of POSS nanoparticles (Hwang et al. 2010). The addition of POSS in the homogenous PI decreases the surface energy of the PI alignment layer and generates the controllable pretilt angle θ_p in a range of $0°<\theta p<90°$ on demand. This method utilizes the conventional PI materials, the manufacture processes and facilities, therefore it can readily be adopted by the current LCD industry.

The pretilt angle of a PI alignment layer can also be controlled by ultra-violet (UV) irradiation (Lu et al., 1996; Yoshida & Koike, 1997; Ichimura, 2000; Chigrinov et al., 2008). UV irradiation on PI alignment films can produce extensive physical and chemical changes, such as photo-isomerization, photo-dimerization and photo-decomposition (Ichimura, 2000; Chigrinov et al., 2008), for PI materials with or without photo-functional groups. Techniques of photo-alignment by polarized and non-polarized UVs had been developed in the 90s and have recently matured for producing large LCDs (Miyachi et al., 2010). UV-modified PI films have also been applied for fabricating LC photonics devices, such as single-cell-gap transflective LCDs and LC Fresnel lens (LCFL) recently (Fan et al., 2004; Jeng et al., 2010; Hwang et al. 2012). The required pretilt angle can be achieved by using UV irradiation for controlling the surface energy of a PI film. Therefore, any LC device requiring patterned alignment areas with different pretilt angles can be obtained by this method.

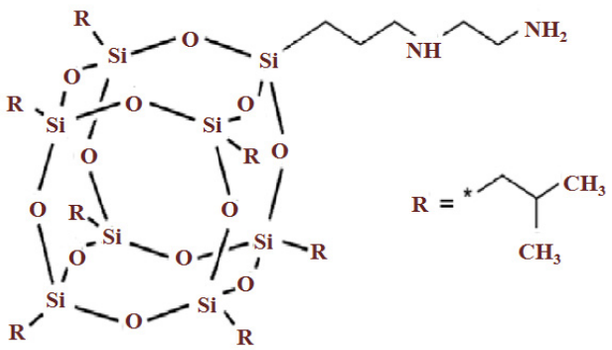

Figure 2. The structure of a PSS-(3-(2-Aminoethyl)amino)propyl-Heptaisobutyl substituted POSS nanoparticle (Sigma-Aldrich Corp., St. Louis, MO, USA).

In this chapter, we reported our developed non-synthetic techniques for controlling the pretilt angles of LC molecules either by doping homogeneous PI with POSS nanoparticles or treating homeotropic PI with UV. The surface energy of POSS-doped PI and UV-treated PI alignment layers were studied to investigate the mechanism of pretilt control. The LC devices, such as no-bias OCB LCDs, LC Fresnel lenses and LC phase gratings, were fabricated and presented in this chapter.

2. Sample preparation

2.1. POSS-doped polyimide

Several commercial homogeneous PI materials from Chimei, Daily Polymer and Nissan Chemical have been tried in the experiments, and some of them work. The POSS nanoparticle, PSS-(3-(2-Aminoethyl)amino)propyl-Heptaisobutyl substituted POSS (SIGMA-ALDRICH) as shown in Fig. 2, was purchased and used in the experiment without further treatment and purification. A powerful ultrasonic processor (S4000, Misonix) for producing the mixture of the POSS/PI was applied for obtaining a good dispersion of 0.2 wt% POSS doped in PI. The mixture was then filtered through a 200 nm syringe filter. The

mixture was further diluted with pure PI in order to generate different concentration of POSS in PI. The POSS/PI films were cast on ITO conducting glass substrates by spin coating at 1000 rpm for 5 s and at 4000 rpm for 60 s. They were then prebaked at 100 °C for 10 minutes and post-baked at 180 °C for 4 hours in a vacuum oven to cure the POSS/PI mixture for forming the alignment layers. The manufacture parameters used here may depend on the PI materials. The surface of the PI alignment layer was then mechanically buffed by using a nylon cloth in such a way that the alignment layer was rubbed once in each direction. Prior to film casting, the ITO glass substrates were cleaned with distilled water, 2-propanol and acetone in an ultrasonic bath and dried at 80 °C for 1 hr.

2.2. UV-treated polyimide

Several commercial homeotropic PI materials from Chimei and JSR have been tried in the experiments, and they required different curing parameters of UV dosage. As shown in Fig. 3, the homeotropic PIs were first spin-coated on the ITO substrates in order to fabricate the UV-treated PI alignment layer. Then, they were pre-baked at 80°C for 10 minutes and post-baked at 210°C for 35 minutes in a vacuum oven. Subsequently, an UV light irradiated the homeotropic PI film through a designed photo mask. For those LC devices requiring precision alignment patterns, the substrates were laminated before UV irradiation as shown in Fig. 3. After finishing UV irradiation, the homeotropic PI film became tilted with a specific pretilt angle. The pretilt can be controlled by the UV dosage, exposure time or intensity. The parameters of UV dosage to reach a specific pretilt angle depended on the PI materials and UV light source. Fig. 4 illustrates a typical UV irradiation spectra used in this work (SP-9,Ushio).

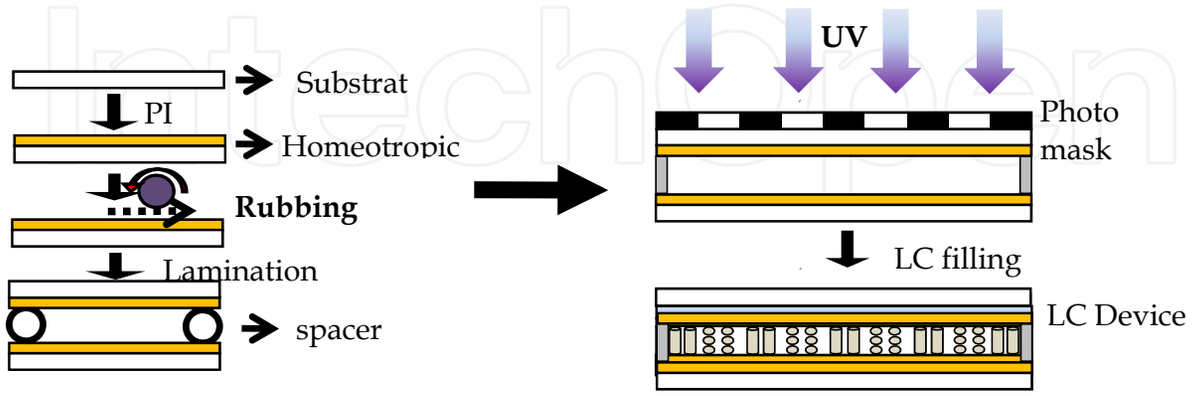

Figure 3. The processes of fabricating an LC device with patterned UV-treated homeotropic PI alignment layers.

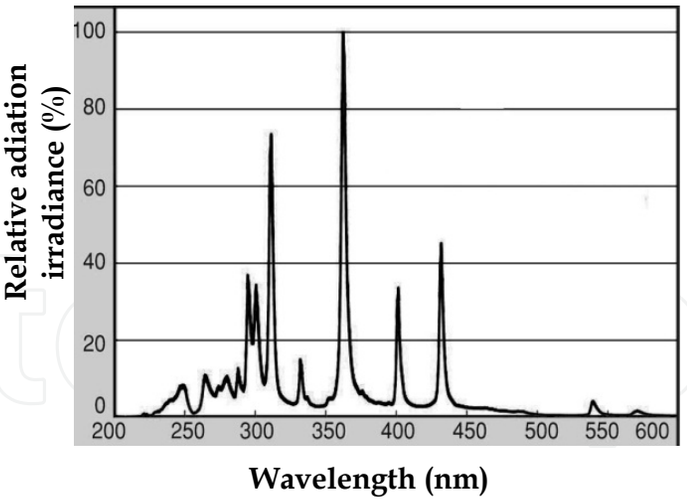

Figure 4. Radiation spectra of an UV light source (SP-9,Ushio).

2.3. Characterization of PI alignment layers

The surface energy of the PI alignment film mainly contributed by the polar part was determined by measuring the contact angle of distilled water on the alignment layers according to the Girifalco-Good-Fowkes-Young model (http://www.firsttenangstroms.com /pdfdocs/SurfaceEnergy.pdf). The contact angle was measured using a contact angle meter (CAM-100, Creating-Nanotech Co.)

To determine the pretilt angle and the polar anchoring energy (PAE) of LC molecules on PI alignment layers, anti-parallel LC test cells were fabricated with a cell gap of ~ 6 μm and were capillary filled with the positive dielectric anisotropic LC molecules (E7, $\Delta\varepsilon$ = 14.1, $\varepsilon_{\perp}$= 5.2, γ=223 mPa.s, K_{33}= 19.5 pN). Several methods have been developed to determine the pretilt angle of LC molecules on PI alignment layers (Baur et al., 1976; Scheffer & Nehring, 1977; Han et al., 1993). Among of them, the crystal rotation method has widely been adopted because of its simple and rapid measurement. However, it is difficult to precisely determine the symmetry point of transmission in the rotation-angle-dependent transmission curve for a LC device with a thin cell gap or a medium pretilt angle. A modified crystal rotation method combined with the common path heterodyne interferometer was used in this work (Hwang & Hsu, 2006; Li et al., 2008). Due to the designed common-path configuration, the phase retardation of the LC cell can be accurately determined in terms of the phase difference of the optical heterodyne signal. The polar anchoring energy (PAE) of the POSS-doped PI and UV-treated PI alignment layers was measured by using the high electric field method (Yu et al., 1999; Nie et al., 2005). Ultraviolet–visible (UV–vis) spectra of PIs were measured with an UV–vis spectrophotometer.

2.4. Fabrication of LC devices

Several LC devices, such as no-bias OCB LC cells, LC Fresnel lenses, and LC phase gratings, requiring medium pretilt angles and patterned pretilt angles were demonstrated.

2.4.1. No-bias OCB LC cells

One traditional low-pretilt OCB LCD using PI without POSS dopant (θ_p~ 2°) and one high-pretilt OCB LCD using PI with 0.05 wt% POSS dopant (θ_p~ 65°) were fabricated for comparison. As shown in Fig. 5, the pretilt angle of an OCB LC cell in the PI alignment layers is in the opposite direction. The cell gap maintained by ball spacers was kept around 5.1 μm in this work**.** The cells were capillary filled with the positive dielectric anisotropic LC molecules E7.

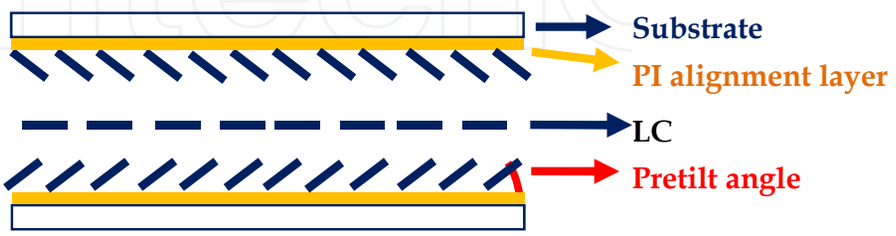

Figure 5. The liquid crystal director configuration in an OCB LC cell.

2.4.2. Fresnel LC Lenses

A binary liquid crystal Fresnel lens (LCFL) can be fabricated by the UV-induced modifications in the pretilt angle of the homeotropic PI films as shown in Fig. 6. An alternating pattern of hybrid-aligned and vertically-aligned LC cells was achieved by irradiating UV on one of the homeotropic PI films through a photo mask with Fresnel zone patterns. Following UV irradiation, the surface of homeotropic PI was modified to become aligned with a specific tilt angle in the even zone areas. The Fresnel zone plate used here is a photo mask with the circular opaque odd zones and transparent even zones. The designed radius r_1 of the innermost zone is 0.4 mm and the radius of the n^{th} zone (r_n) is given by $r_n^2 = nr_1^2$, where n is the zone number. The Fresnel zone plate has 100 zones in approximately a 1 cm aperture, and it has a primary focal length f ~25 cm at λ= 632.8 nm.

As shown in Fig. 6, the polarization-dependent and polarization-independent LCFLs can be fabricated by buffing the UV-treated PI films horizontally and circularly, respectively. Both buffed top (homeotropic PI) and bottom ITO glass substrates (UV-treated homeotropic PI) were then assembled into an LC cell with a cell gap of ~10 μm maintained by spacers. The positive LC material (E7) was then injected into the empty cell.

The image quality and voltage-dependent diffraction efficiency of the LCFLs were measured by using an expanded He-Ne laser light source to approximately 1 cm in diameter corresponding to the active area of the LCFLs as shown in Fig. 7. The first-order diffraction efficiency is defined as the ratio of the first-order diffraction intensity at the primary focal point to the total transmitted intensity through the LCFL. The polarization direction of the incident light with respect to the horizontal buffing direction of the LCFLs was tuned by a linear polarizer and a half wave plate. The focusing properties of the LCFL were recorded by using a CCD camera or a detector, set ~25 cm from the LCFLs.

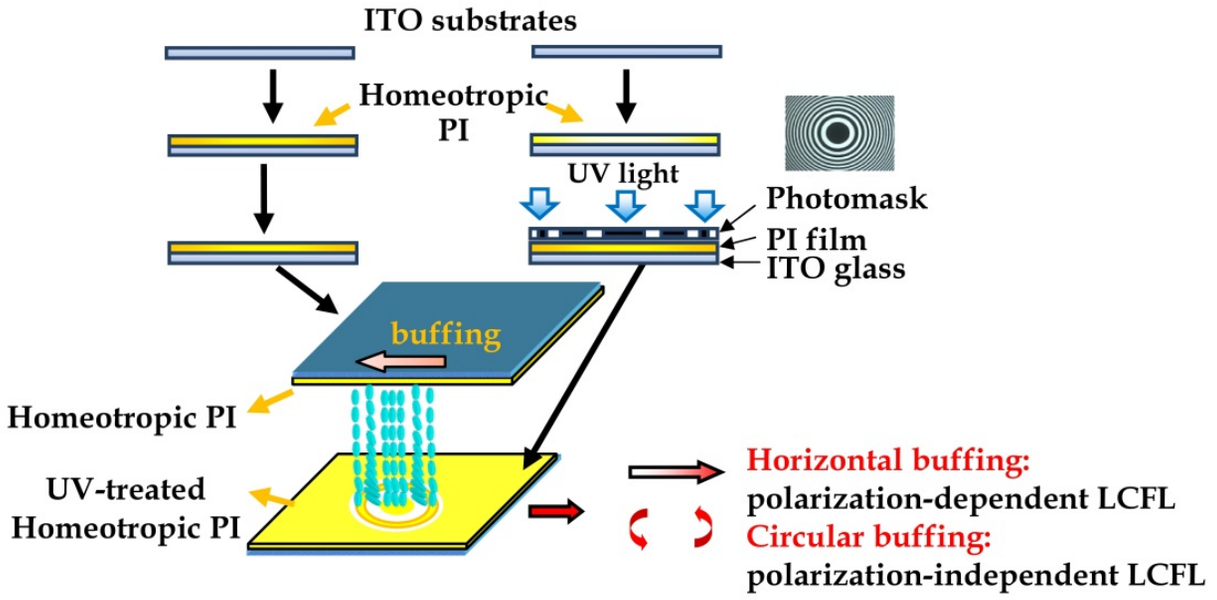

Figure 6. The fabrication process of the LC Fresnel lenses.

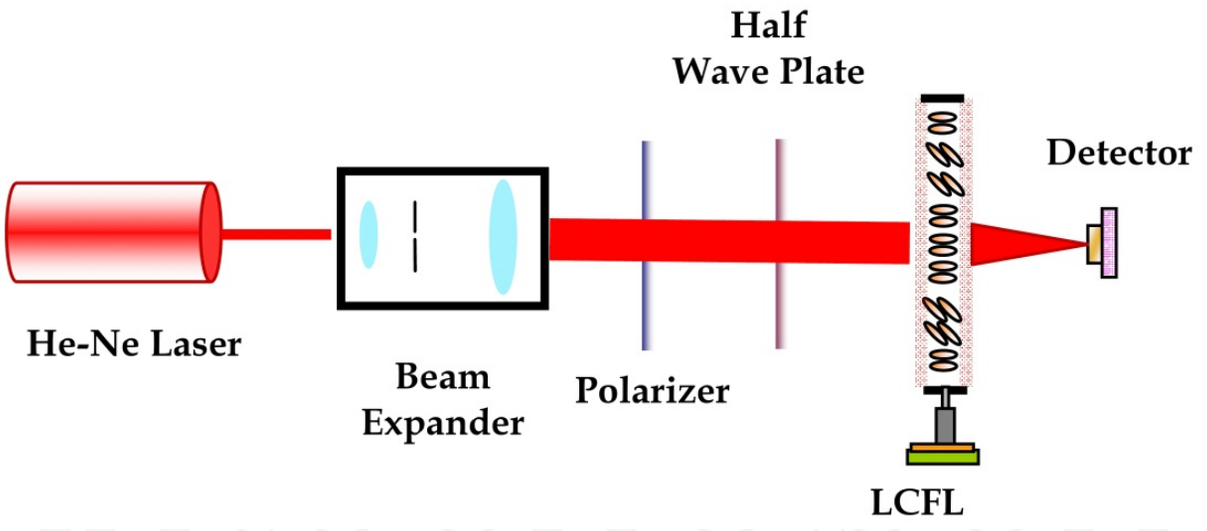

Figure 7. The experimental setup for measuring the focus properties of the LC Fresnel lens.

2.4.3. LC Phase gratings

In order to fabricate an LC phase grating, the laminated empty LC cell was irradiated by UV through a photo mask with the spacing around 200 μm in this work as shown in Fig. 3 and Fig. 8. The empty LC cell shows a strong UV absorption for the wavelength less than 300 nm due to the ITO glasses and PI materials, therefore the wavelength of UV irradiation between 300 nm and 400 nm is used for photo-decomposition of homeotropic PIs. The positive LC material (E7) was then injected into the empty cell for being an LC phase grating.

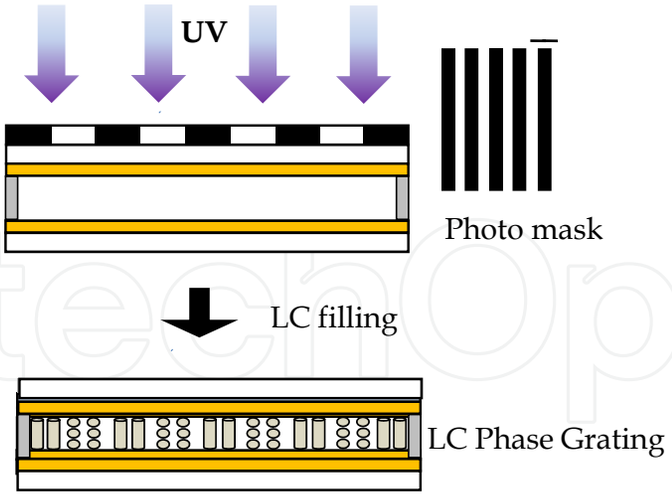

Figure 8. The fabrication process of the liquid crystal phase grating.

3. Results and discussion

3.1. Characteristics of PIs

The results of the surface energy of the POSS-doped PI alignment layer with different POSS wt% doped in PI and the UV-treated PI with different UV irradiation dosage are shown in Fig 9 and Fig. 10, respectively. They both indicate that the pretilt angles of LC molecules depend on the surface energy of the PI alignment layers. As shown in Fig. 9, the addition of POSS nanoparticles in the homogeneous PI mediates and lowers the surface energy of the PI alignment layer. However, the irradiation of UV on homeotropic PI mediates and increases the surface energy of the PI alignment layer as shown in Fig. 10. The pretilt angles of the rubbed PI films are continuously decrease with increasing surface energy as shown in Fig. 9 and Fig. 10 for POSS-doped PI and UV-treated PI alignment layers, respectively. The influence of surface energy of PI alignment layers on pretilt angles had been investigated (Paek et al., 1998; Yu et al., 1999; Ban & Kim, 1999). It showed that an alignment layer with higher surface energy gives the lower pretilt angle due to the increased attractive strength between LC molecules and molecules of the alignment layers.

The PAEs of the homogeneous PI alignment layer doped with different POSS concentration and the homeotropic PI alignment layer irradiated with different UV dosage are shown in Fig. 11 and Fig. 12, respectively. As shown in Fig. 11, the PAE is almost constant around 2.4×10^{-4} J/m^2 regardless of the POSS concentration doped in PI. As shown in Fig. 12, The PAE increases from 1.3×10^{-4} J/m^2 to 5.5×10^{-4} J/m^2 as the dosage of UV irradiation increases to 88 J/cm^2. It indicates the anchoring strength of UV-treated PI films is not degraded by UV irradiation and it may depend on the surface energy of the UV-treated PI. The feature of increased PAE of the UV-treated PI film from homeotropic alignment to homogeneous alignment deserves further study. The novel methods of pretilt control by addition of POSS in homogenous PI and photo-irradiation of homeotropic PI are applicable to fabrication of LCDs requiring a specific pretilt angle with moderate PAE.

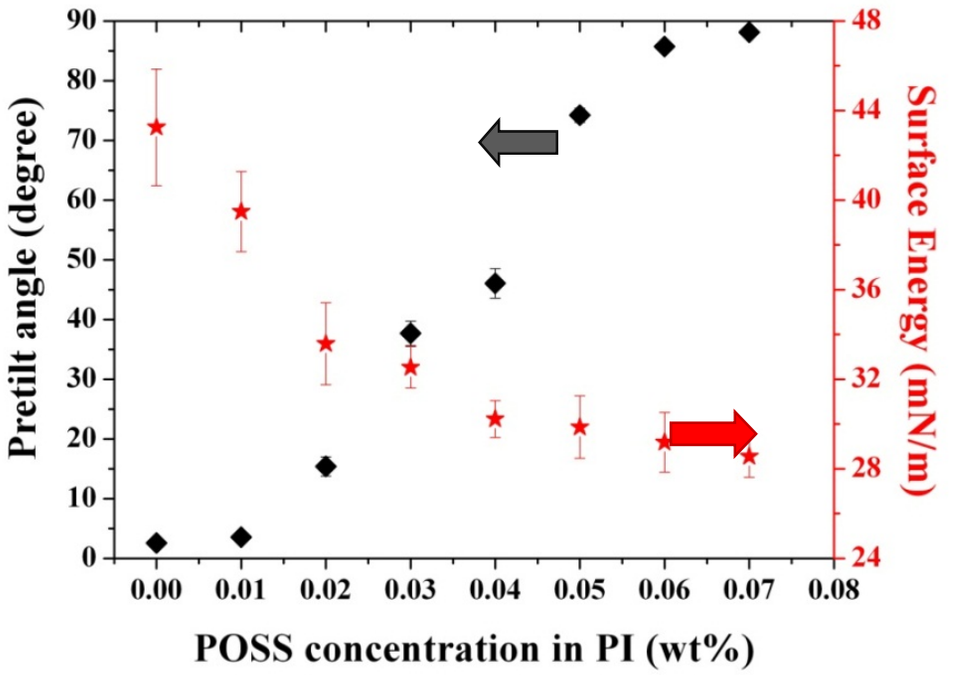

Figure 9. Pretilt angle and surface energy of POSS/PI alignment layers as a function of POSS concentration in PI.

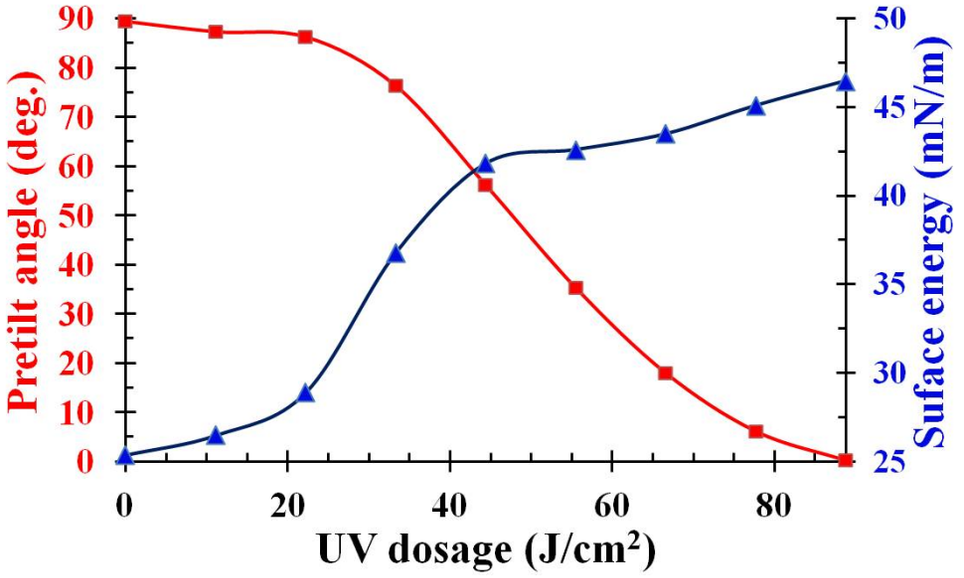

Figure 10. Pretilt angle and surface energy of the UV-treated homeotropic PI alignment layer as a function of UV dosage (Hwang et al. 2012).

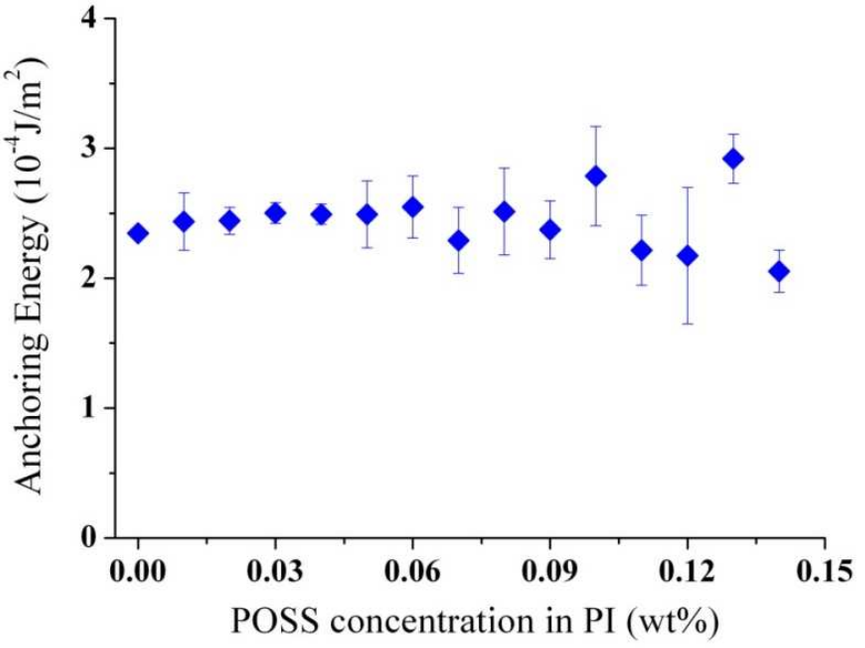

Figure 11. Polar anchoring energy of POSS/PI alignment layers as a function of POSS concentration doped in homogeneous PIs (Hwang et al. 2010).

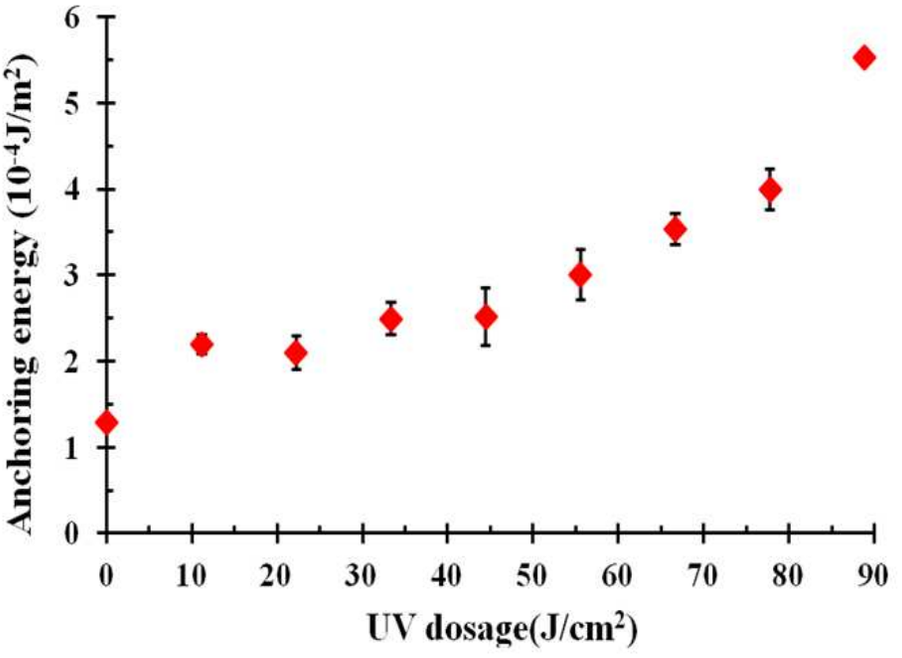

Figure 12. Polar anchoring energy of the homeotropic PI alignment layer as a function of UV dosage (Hwang et al. 2012).

The UV–vis spectra of the POSS doped PIs and UV-treated PIs are shown in Fig. 13 and Fig. 14, respectively. They both show good transparency in the visible range. There is no significant difference in UV-Vis spectra for 0.07 wt % POSS doped in PI as shown in Fig. 13. However, there is a significant increase in absorption and a small blue shift of absorption peak for the UV-irradiated PI film as shown in Fig. 14. It may indicate that the compositions

of PIs are changed with UV irradiation. Further investigations, such as FT-IR spectra, may reveal the detailed information.

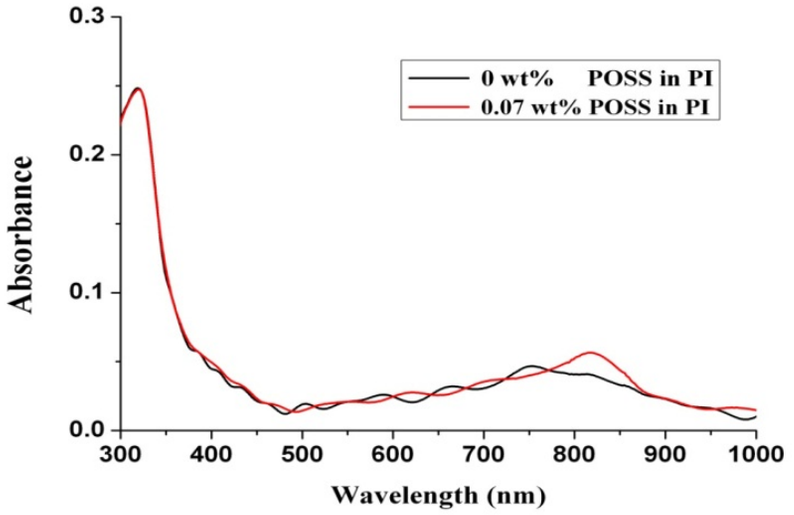

Figure 13. UV-vis spectra of the homogenous PI films with and without POSS dopant.

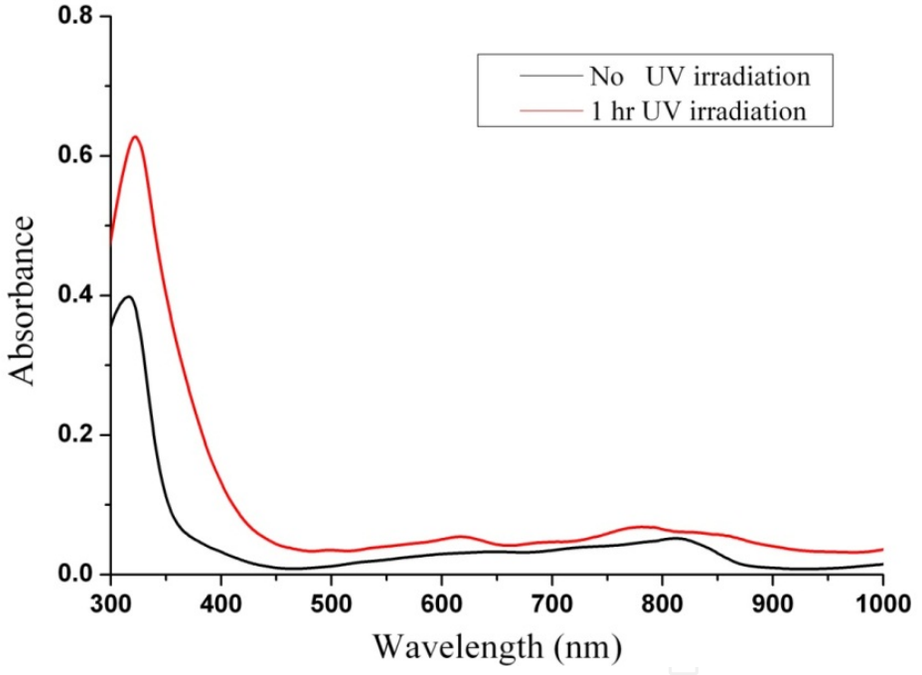

Figure 14. UV-vis spectra of the PI films with and without UV irradiation.

3.2. No-bias OCB results

The transient behaviors of the conventional low-pretilt OCB LC cell and the high-pretilt OCB LC cell under different applied voltages and finally relaxing the bias voltage observed by a polarized optical microscopy (POM) are shown in Fig. 15(a) and Fig. 15(b), respectively. The cell becomes totally dark when applying 10 V for reaching the homeotropic state. The transition from the bend state to the homeotropic state and the subsequent return from the

homeotropic state to the initial bend state occur immediately for the high-pretilt OCB LC cell as shown in Fig. 15(b). No intermediate transition modes occur for the high-pretilt OCB LC cell when compared with the low-pretilt OCB LC cell. As a result, our demonstrated high-pretilt POSS-doped PI alignment layer stabilizes the bend state deformation of an OCB LC cell even at zero bias voltage.

The voltage dependent transmission properties of the conventional low-pretilt and the high-pretilt OCB LCDs were measured as shown in Fig. 16, by applying forward voltage (0V to 10 V) and backward voltage (10V to 0 V) where there was no bias voltage applied on the OCB LCDs and the data were recorded for one second at the first second after the voltage was applied. Due to the energy gap between the splay and bend state of a traditional low-pretilt OCB LCD, some transient time (warm-up time) is required between those two states, and that is the reason that the forward voltage dependent transmission curve does not match with the backward voltage one as shown in Fig. 16. The high-pretilt OCB LC cell could overcome the energy barrier and show a better electro-optical property than the low-pretilt one.

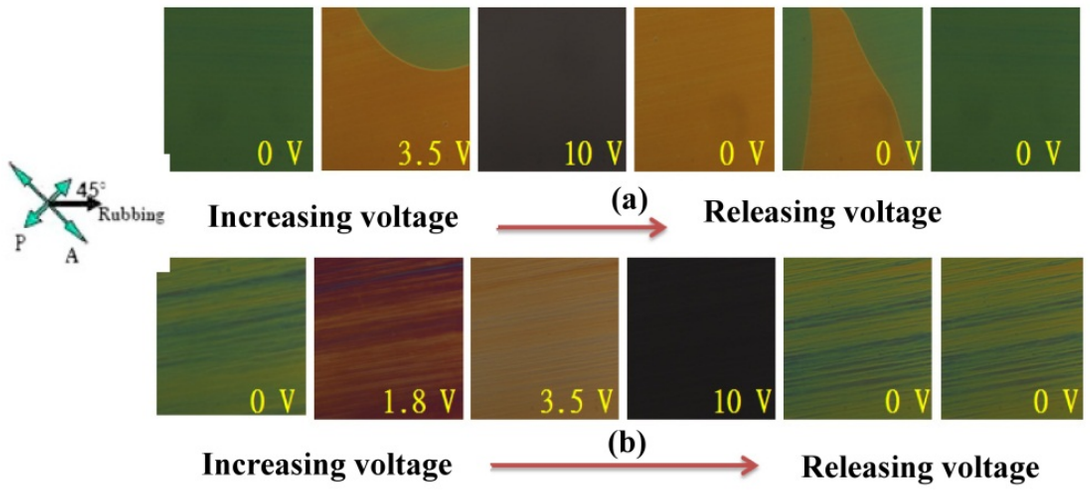

Figure 15. Photographs observed by a polarized optical microscopy. (a) The low-pretilt OCB LC cell and (b) the high-pretilt OCB LC cell under different applied voltages.

The switching properties of the no-bias high-pretilt OCB LC cell with 0.05 wt% POSS doped in PI is shown in Fig. 17 with a driving voltage from 0V to 5V. It can be seen that the switching time of 0.8 ms from bend state to homeotropic state and the relaxation time of 1.5 ms from homeotropic state to bend-state are shown.

3.3. LC Fresnel Lens

The results of the voltage-dependent first-order diffraction efficiency of a polarization-dependent LCFL and a polarization-independent LCFL with linear polarization of the incident light at θ=0°, 45° and 90°, with respect to the buffing direction of PI alignment layer are shown in Fig. 18 and Fig. 19, respectively. The diffraction efficiency of a polarization-dependent LCFL progressively increases to the maximum diffraction efficiency ~ 35% at V

=1.1 V with the linear polarization of the incident light at θ=0° as shown in Fig. 18. The characteristics of the polarization-independent LCFL are shown in Fig. 19, and the maximum diffraction of ~22 % is obtained at ~ 1.2 V regardless of polarization of the incident light. In order to characterize the imaging qualities of the LCFL as function of applied voltage, an expanded He-Ne laser was used as the object, and the focusing images shown in Fig. 20 were recorded with the CCD camera located at focus point, 25 cm behind the LCFL.

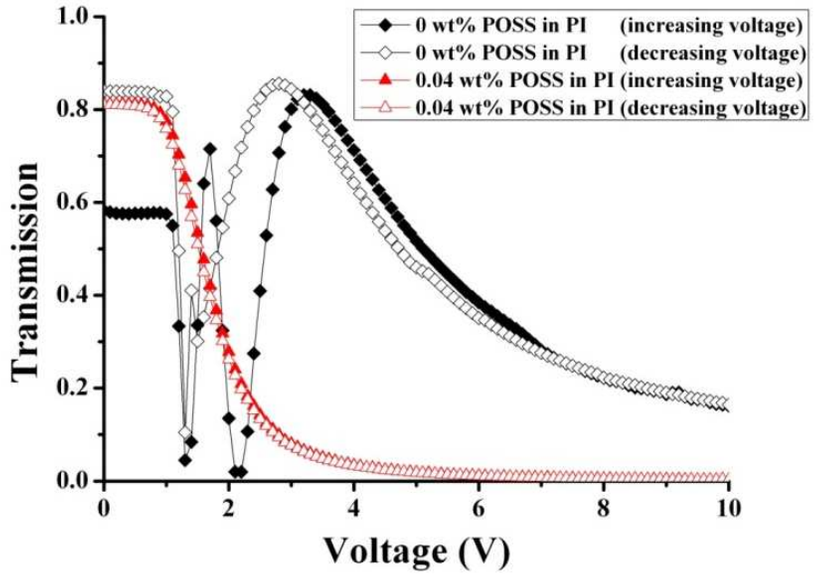

Figure 16. Voltage dependent transmission curves of the traditional low-pretilt and the high-pretilt OCB LC cells by applying forward (0 V to 10 V) and backward (10 V to 0V) voltages.

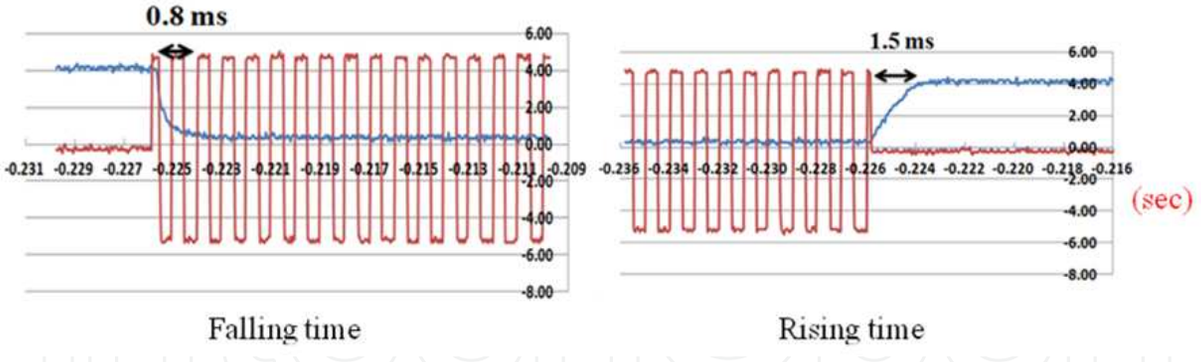

Figure 17. Switching time of the no-bias OCB LC cell.

3.4. LC Phase grating

The tunable diffraction grating has been found in many applications for photonics, such as optical information processing and telecommunication applications. The images of the LC phase grating observed by a POM are shown in Fig. 21. As shown in Fig. 21(a), the dark regions correspond to vertically-aligned LC on PI without UV treatment, and the bright regions correspond to planar-aligned LC on PI with UV treatment. The first-order diffraction efficiency of the LC phase grating as a function of the applied voltage is shown in

Fig. 22. The first-order diffraction efficiency of a phase grating is determined by the relative phase difference between the UV-irradiated and the non UV-irradiated regions of PI alignment layers. If the direction of polarization is parallel to the grating, the phase grating has maximum diffraction efficiency. The diffraction efficiency decreases gradually to zero as the voltage increases, because all of the LC directors are reoriented almost perpendicular to the substrates.

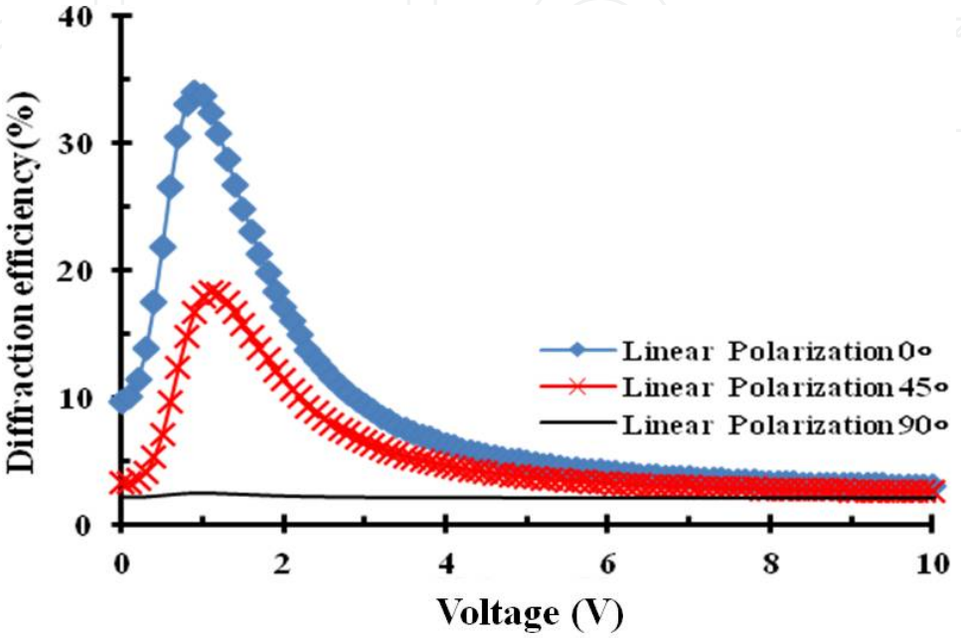

Figure 18. The voltage-dependent diffraction efficiency of a polarization-dependent LC Fresnel lens (Hwang et al. 2012).

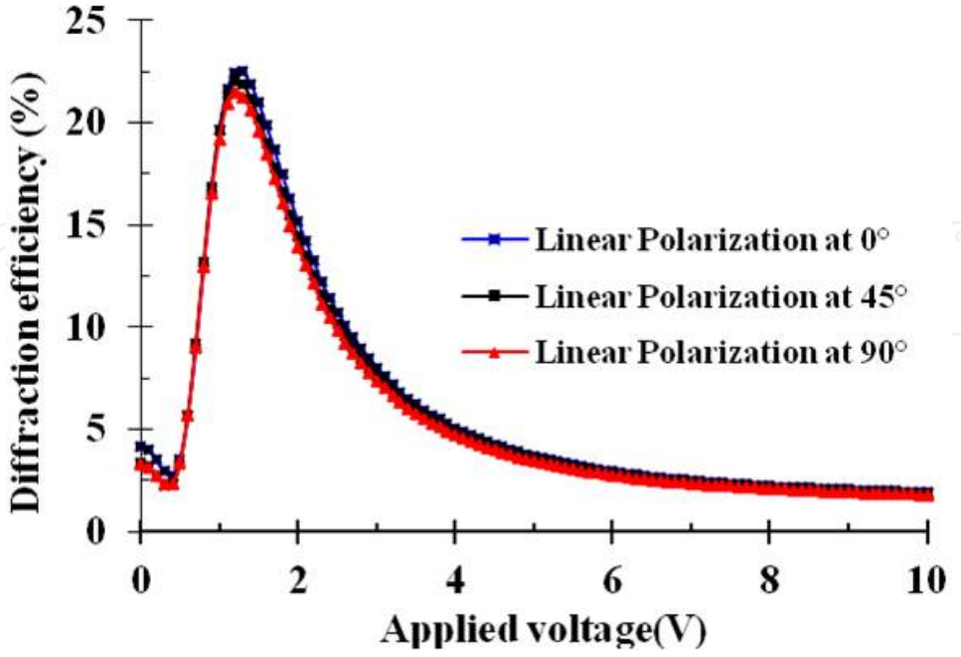

Figure 19. The voltage-dependent diffraction efficiency of the polarization-independent LC Fresnel lens (Hwang et al. 2012).

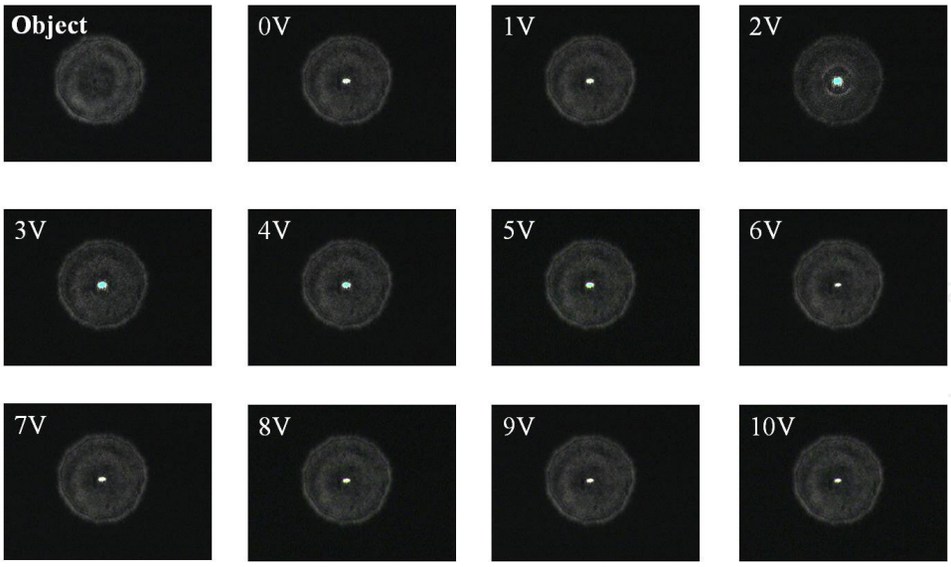

Figure 20. Focusing images of the LC Fresnel lens with different driving voltage recorded by a CCD camera at focal point.

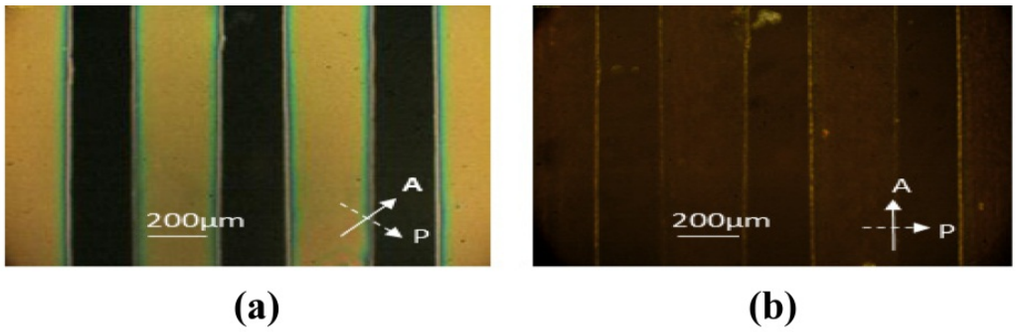

Figure 21. The images of the LC phase grating observed by a POM.

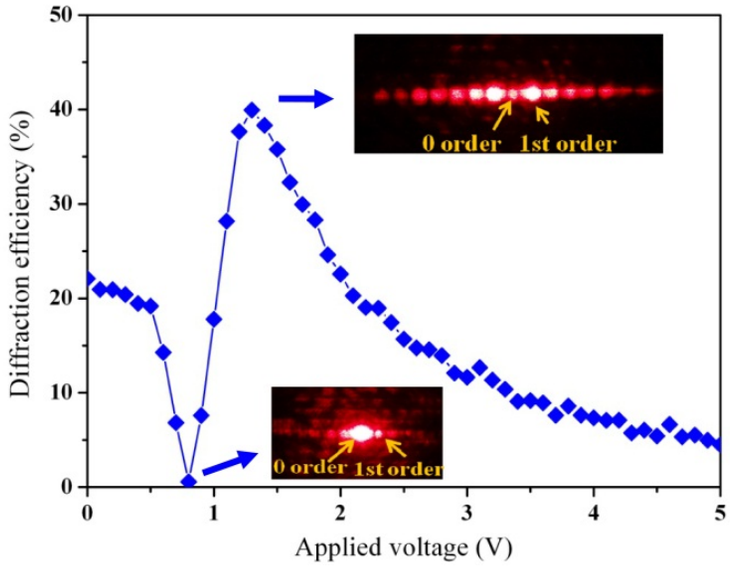

Figure 22. The first-order diffraction efficiency as a function of the applied voltage. Two insets of the diffraction patterns are shown at V=0.8V and V=1.3 V, respectively.

4. Conclusion

We have developed two approaches for controlling the pretilt angle of the PI alignment layers by using the conventional PI materials. The proposed methods are compatible with current methods familiar in the LCD industry. The LC devices, such as no-bias OCB LC cells, LCFLs and LC phase gratings, are demonstrated in this chapter by using the proposed techniques. A future study should examine the long-term thermal stability of these modified PI films.

Author details

Shie-Chang Jeng
Institute of Imaging and Biomedical Photonics, National Chiao Tung University, Taiwan

Shug-June Hwang
Dep. of Electro-Optical Engineering, National United University, Taiwan

Acknowledgement

The authors would like to thank the National Science Council of Taiwan for financially supporting this research under contracts: NSC 98-2112-M-009-020-MY2, NSC 98-2221-E-239-003-MY2, NSC 99RC04, and NSC 100-2112-M-009 -014 -MY3. The authors are grateful to Dr. Huai-Pin Hsueh from Chimei for supporting PI materials and helpful discussions and to I-Ming Hsieh, Tai-An Chen, Han-Shiang Liu and Mu-Zhe Chen for their help with the experiments.

5. References

Acosta, EJ, Towler, MJ & Walton, HG (2000). The role of surface tilt in the operation of pi-cell liquid crystal devices," *Liquid Crystals*, Vol. 27, No. 7, (Aug), pp. 977-984.

Ahn, D, Jeong, YC, Lee, S, Lee, J, Heo, Y & Park, JK (2009). Control of liquid crystal pretilt angles by using organic/inorganic hybrid interpenetrating networks. *Optics Express*, Vol. 17, No. 19, (Sep), pp. 16603-16612.

Ban, BS & Kim, YB (1999). Surface Free Energy and Pretilt Angle on Rubbed Polyimide Surfaces. *Journal of Applied Polymer Science,* Vol. 74, No. 2, (Oct), pp. 267-271.

Baur, G, Wittwer, V & Berreman, DW (1976). Determination of the tilt angles at surfaces of substrates in liquid crystal cells. *Physics Letters A,* Vol. 56, No. 2, (Mar), pp. 142-144.

Chen, TJ & Chu, KL (2008). Pretilt angle control for single-cell-gap transflective liquid crystal cells, *Applied physics letters,* Vol. 92, No. 9, (Mar), pp. 091102.

Chigrinov, VG, Kozenkov, VM & Kwok, HS (July 22, 2008). *Photoalignment of Liquid Crystalline Materials: Physics and Applications*, John Wiley & Sons Ltd, ISBN: 0470065397, West Sussex.

Fan, YY, Chiang, HC, Ho, TY, Chen, YM, Hung, YC, Lin, IJ, Sheu, et al. (2004). A Single-Cell-Gap Transflective LCD. *SID Symposium Digest of Technical Papers*, Vol. 35, No. 1, (May), pp. 647-649.

Han, KY, Vetter, P & Uchida, T (1993). Determination of molecular inclination in rubbed polymer for liquid crystal alignment by measuring retardation. *Japanese Journal of Applied Physics,* Vol. 32, No. 9A, (Sep), pp. L1242–L1244.

Hwang, SJ & Hsu, MH (2006). Heterodyne method for determining the surface tilt angle of nematic liquid-crystal displays. *Journal of the Society for Information Display*, Vol. 14, No. 11, (Nov), pp. 1039-1043.

Hwang, SJ, Jeng, SC, Yang, CY, Kuo, CW & Liao, CC (2009). Characteristics of nanoparticle-doped homeotropic liquid crystal devices. *Journal of Physics, D* Vol. 42, No. 2, (Jan), pp. 025102.

Hwang, SJ, Jeng, SC, & Hsieh IM (2010). Nanoparticle-doped polyimide for controlling the pretilt angle of liquid crystals devices. *Optics Express,* Vol. 18, No, 16, (Aug), pp. 16507-16512.

Hwang, SJ, Chen, TA, Lin, KR, & Jeng, SC (2012). Ultraviolet light treated polyimide alignment layers for polarization-independent liquid crystal Fresnel lenses. *Applied Physics B,* Vol. 107, No. 1, (Apr),pp.151–155.

Ichimura, K (2000). Photoalignment of liquid-crystal systems. *Chemical Reviews*, Vol. 100, No. 5, (May), pp. 1847-1874.

Janning, JL (1972). Thin film surface orientation for liquid crystals. *Applied physics letters,* Vol. 21, No. 4, (May), pp. 173.

Jeng, SC, Kuo, CW, Wang, HL & Liao, CC (2007). Nanoparticles-induced vertical alignment in liquid crystal cell. *Applied physics letters,* Vol. 91, No. 6, (Aug), pp. 061112.

Jeng, SC, Hwang, SJ, Horng, JS & Lin, KR (2010). Electrically switchable liquid crystal Fresnel lens using UV-modified alignment film. *Optics Express,* Vol. 18, No, 25, (Dec), pp. 26325-26331.

Komitov, L (2008). Tuning the alignment of liquid crystals by means of nano-structured surfaces. *Journal of the Society for Information Display*, Vol. 16, No. 9, (Sep), pp. 919-925.

Li, YW, Ho, JYL, Yeung, FSY & Kwok, HS (2008). Simultaneous determination of large pretilt angles and cell gap in liquid crystal displays. *Journal of Display Technology,* Vol. 4, No. 1, (Mar), pp. 13–17.

Lee, YJ, Gwag, JS, Kim, YK, Jo, SI, Kang, SG, Park, YR & Kim, JH (2009). Control of liquid crystal pretilt angle by anchoring competition of the stacked alignment layers. *Applied physics letters,* Vol. 94, No. 4, (Jan), pp. 041113.

Lu, J, Deshpande, SV, Gulari, E, Kanickia, J & Warren, WL (1996). Ultraviolet light induced changes in polyimide liquid-crystal alignment films. *Journal of Applied Physics,* Vol. 80, No., (Jul), pp. 5028-5034.

Miyachi, K, Kobayashi, K, Yamada, YY & Mizushima, S (2010). The World's First Photo Alignment LCD Technology Applied to Generation Ten Factory. *SID Symposium Digest of Technical Papers*, Vol. 41, No. 1, (May), pp. 579-582.

Nastishin, YA, Polak, RD, Shiyanovskii, SV, Bodnar, VH & Lavrentovich, OD (1999). Nematic polar anchoring strength measured by electric field techniques. *Journal of Applied Physics,* Vol. 86, No. 8, (Oct), pp. 4199-4213.

Nie, X, Lin, YH, Wu, TX, Wang, H, Ge, Z & Wu, ST (2005). Polar anchoring energy measurement of vertically aligned liquid-crystal cells. *Journal of Applied Physics,* Vol. 98, No. 1, (Jul), pp. 013516.

Nishikawa, M (2000). Design of Polyimides for Liquid Crystal Alignment Films. *Polymers for Advanced Technologies*, Vol. 11, No. 8-12, (Nov), pp. 404–412.

Paek, SH, Duming, CJ, Lee, KW & Lien, A (1998). A mechanistic picture of the effects of rubbing on polyimide surfaces and liquid crystal pretilt angles. *Journal of Applied Physics*, Vol. 83, No. 3, (Sep), pp. 1270-1280.

Scheffer, TJ & Nehring, J (1977). Accurate determination of liquid-crystal tilt bias angle. *Journal of Applied Physics,* Vol. 48, No. 5, (May), pp. 1783–1792.

Tsuda, Y (2011). Polyimides Bearing Long-Chain Alkyl Groups and Their Application for Liquid Crystal Alignment Layer and Printed Electronics, *Features of Liquid Crystal Display Materials and Processes,* Natalia V. Kamanina, pp. 4-24, InTech, ISBN: 978-953-307-899-1.

Uchida, T, Ohgawara, M & Wada, M (1980). Liquid Crystal Orientation on the Surface of Obliquely-Evaporated Silicon Monoxide with Homeotropic Surface Treatment. *Japanese Journal of Applied Physics,* Vol. 19, No. 11, (Nov), pp. 2127-2136

Vaughn, KE, Sousa, M, Kang, D and Rosenblatt, C (2007). Continuous control of liquid crystal pretilt angle from homeotropic to planar. *Applied physics letters,* Vol. 90, No. 19, (May), pp. 194102.

Wu, WY, Wang, CC & Fuh, AYG (2008). Controlling pre-tilt angles of liquid crystal using mixed polyimide alignment layer. *Optics Express*, Vol. 16, No. 21, (Oct), pp. 17131-17137.

Xiao, S, Nguyen, M, Gong, X, Gao, Y, Wu, H, Moses, D & Heeger, AJ (2003). Stabilization of Semiconducting Polymers with Silsesquioxane. *Advanced Functional Materials,* Vol. 13, No. 1, (Jan), pp. 25–29.

Yei, DR, Kuo, SW, Su, YC & Chang, FC (2004). Enhanced thermal properties of PS nanocomposites formed from inorganic POSS-treated montmorillonite. *Polymer,* Vol. 45, No. 8, (Apr), pp. 2633-2640.

Yeung, FS & Kwok, HS (2006).Fast-response no-bias-bend liquid crystal displays using nanostructured surfaces, *Applied physics letters*, Vol. 88, No. 6, (Feb), pp. 063505.

Yeung, FS, Ho, JY, Li, YW, Xie, FC, Tsui, OK, Sheng, P & Kwok, HS (2006). Variable liquid crystal pretilt angles by nanostructured surfaces. *Applied physics letters,* Vol. 88, No. 8, (Jan), pp. 051910.

Yoshida, H & Koike, Y (1997). Inclined homeotropic alignment by irradiation of unpolarized UV light. *Japanese Journal of Applied Physics,* Vol. 36, No. 4A, (Feb), pp. L428-L431.

Yu, XJ & Kwok, HS (2004). Bistable bend-splay liquid crystal display. *Applied physics letters,* Vol. 85, No. 17, (Aug), pp.3711.